Robustness of predator-prey models for confinement regime transitions in fusion plasmas

H. Zhu, S. C. Chapman, and R. O. Dendy

Robustness of predator-prey models for confinement regime transitions in fusion plasmas

H. Zhu,[1] S. C. Chapman,[1,2] and R. O. Dendy[3,1]

[1]*Department of Physics, Centre for Fusion, Space and Astrophysics, University of Warwick, Coventry CV4 7AL, United Kingdom*
[2]*Department of Mathematics and Statistics, University of Tromso, Norway*
[3]*Euratom/CCFE Fusion Association, Culham Science Centre, Abingdon, Oxfordshire OX14 3DB, United Kingdom*

Energy transport and confinement in tokamak fusion plasmas is usually determined by the coupled nonlinear interactions of small-scale drift turbulence and larger scale coherent nonlinear structures, such as zonal flows, together with free energy sources such as temperature gradients. Zero-dimensional models, designed to embody plausible physical narratives for these interactions, can help to identify the origin of enhanced energy confinement and of transitions between confinement regimes. A prime zero-dimensional paradigm is predator-prey or Lotka-Volterra. Here, we extend a successful three-variable (temperature gradient; microturbulence level; one class of coherent structure) model in this genre [M. A. Malkov and P. H. Diamond, Phys. Plasmas **16**, 012504 (2009)], by adding a fourth variable representing a second class of coherent structure. This requires a fourth coupled nonlinear ordinary differential equation. We investigate the degree of invariance of the phenomenology generated by the model of Malkov and Diamond, given this additional physics. We study and compare the long-time behaviour of the three-equation and four-equation systems, their evolution towards the final state, and their attractive fixed points and limit cycles. We explore the sensitivity of paths to attractors. It is found that, for example, an attractive fixed point of the three-equation system can become a limit cycle of the four-equation system. Addressing these questions which we together refer to as "robustness" for convenience is particularly important for models which, as here, generate sharp transitions in the values of system variables which may replicate some key features of confinement transitions. Our results help to establish the robustness of the zero-dimensional model approach to capturing observed confinement phenomenology in tokamak fusion plasmas. © 2013 AIP Publishing LLC.
[http://dx.doi.org/10.1063/1.4800009]

I. INTRODUCTION

Energy transport in toroidal magnetically confined fusion plasmas is determined, in most cases, by the effects of small-scale turbulence and larger scale coherent nonlinear structures, together with their mutual interactions. These structures include zonal flows and geodesic acoustic modes,[1–7] which are radially localised poloidal flows, and streamers,[8] which are radially highly elongated and poloidally localised. The importance of these structures for energy transport was highlighted in large scale numerical simulations,[9,10] and the first direct experimental observation of streamers was reported in 2008.[8] Zonal flows have been the subject of extensive theoretical and observational work.[1–7] There is now substantial experimental support for the long-standing hypothesis[11] that the growth of zonal flows is driven by the averaged Reynolds stress of small scale turbulence. The latter can be locally suppressed by the resultant shear flow, thereby generating a temporally quasi-discontinuous enhancement of global energy confinement: the L-H transition.[12] Whether zonal flows or streamers are preferentially formed under specific plasma conditions, and how they compete, has been addressed from various perspectives,[13–15] and remains an open question. For a recent review of

experimental observations of the interaction between meso-scale structures (such as zonal flows and streamers) and microscale structures (such as drift turbulence), see Ref. 16; of drift turbulence, particularly in relation to transitions in global confinement, see Ref. 17; and of the L-H transition, see Ref. 18. A recent review of these physics issues in a broad context is provided by Ref. 19. As emphasised in Refs. 16–19 and references therein, recent diagnostic advances are transforming the experimental study of time evolving micro-turbulence and coherent nonlinear mesoscale structures during confinement transitions. This generates fresh theoretical challenges. In addition, the ability to understand and control this plasma physics phenomenology will be central to the successful operation of the next step magnetic confinement fusion experiment ITER.[20]

It is remarked by Malkov and Diamond in Ref. 21, here-after referred to as MD, that transport models derived from the fundamental equations of plasma physics continue to add much to our understanding but "tend to be increasingly, if not excessively, detailed. Therefore, there is high demand for a simple, illustrative theoretical model with a minimal number of critical quantities responsible for the transition. Such models usually yield or encapsulate basic insight into complicated phenomena." One approach in fusion plasmas is

that of zero-dimensional models for the interaction between microturbulence and coherent nonlinear structures, in particular predator-prey or Lotka-Volterra.[22,23] The properties of Lotka-Volterra systems, both mathematically and from the perspective of fusion plasma physics, are by no means fully explored and remain an active field of research.[24–29] For fusion applications, a key step is to establish agreement between the outputs of such models and the observed confinement phenomenology, which should ideally extend to the character of measured time traces of key properties near transitions, for example. Recent experimental results[31,32] are encouraging in this respect. There is an important additional requirement. The zero-dimensional models used for this application should be robust, in the sense that the character of their outputs remains largely invariant against minor changes in the formulations of the models. This requirement for robustness has been explicitly noted[33] in the other main class of zero-dimensional heuristic model for magnetised plasma confinement, namely, sandpiles, both in fusion[34–40] and in solar-terrestrial[33,41–43] contexts, and requires investigation for predator-prey and Lotka-Volterra applications to fusion plasmas.

There are several aspects to the degree of invariance of the phenomenology generated by a zero-dimensional model when aspects of the model are changed. First, what is the long-time behaviour of the system and how sensitive is this to variation in the model parameters?[44,45] Second, how sensitively does the nature of the system's evolution towards its final state depend on the initial conditions? Is there an attractive fixed point or limit cycle towards which the system flows as time passes? If so, what is its basin of attraction? Third, how sensitive is the path to this attractor? This is particularly important for models which, as here, generate sharp transitions in the values of system variables which may replicate some key features of confinement transitions in tokamaks. If the initial conditions are varied, is the time at which the transition occurs delayed or brought forward, or does its character change, for example? Further, given two zero-dimensional models which are schematically distinct but adjacent, how similar is the phenomenology of their solutions? An example is provided here by our extension of the model of MD[21] to incorporate two variables, rather than one, representing different classes of large scale coherent nonlinear field, in a four-variable system. The case of two predators and one prey was considered theoretically in the model of Itoh and Itoh,[29] hereafter referred to as II, and by Miki and Diamond,[30] and there is recent experimental motivation.[31,32] Insofar as a zero-dimensional model turns out to be robust with respect to the considerations outlined (attractors; initial conditions; structural adjacency), confidence is strengthened in the mapping from model variables to specific plasma properties, and from the time evolving behaviour of the model to that of the plasma system.

In the present paper, we focus from this perspective on the interesting and successful mathematical model proposed in MD. This is constructed in terms of variables representing the magnitude of the plasma temperature gradient and the amplitudes of small scale drift turbulence and of large scale coherent nonlinear structures such as zonal flows. Malkov

and Diamond proposed[21] certain mappings between different solution regimes of their model and different confinement regimes of tokamak plasmas. In the interest of continuity, we follow the confinement regime nomenclature of MD in relation to model outputs in the present paper. We investigate the robustness of the phenomenology of the MD model extended as described, for parameter regimes identical, or adjacent, to those used in the key figures of MD. Where robustness is demonstrated and, if possible, explained, this reinforces confidence that models in the genre of MD and II may capture key features of the physics of confinement transitions in tokamak plasmas.

II. MODEL EQUATIONS

Specifically, the MD model is a closed system of nonlinear differential equations which couple the time evolution of three variables: the drift wave-driving temperature gradient N, the energy density of drift wave turbulence E, and the zonal flow velocity U. The three variables of the II model exclude N, retain drift turbulence energy density denoted by W, and incorporate the energy densities of two competing classes of coherent nonlinear structure, zonal flows Z and zonal fields (e.g., streamers) M. Miki and Diamond[30] introduced a zero-dimensional three-variable two-predator, one prey model, where the predators are identified with zonal flows and geodesic acoustic modes. The aspect of robustness which we first address can therefore be expressed in physical terms as follows. We adopt the philosophy of II and of Ref. 30 by introducing two competing classes of coherent nonlinear structure, here identified with zonal flows and streamers, which replace the single class in MD. The other two MD equations are adjusted only so far as necessary to accommodate these two fields, instead of one, in a mathematically symmetrical way as in II. We investigate how far the model outputs of our new four-variable system differ from those of the three-variable system of MD. A good focus for this study is provided by the time traces captured in Figs. 2–4 of MD, which have been mapped to transitions observed between tokamak confinement regimes. How are these traces altered by the inclusion of a second competing class of coherent nonlinear structure? The answers to these questions are conditioned by the underlying phase space structure of families of solutions to the models, as plotted in Fig. 5 of MD, for example. In addition to studying time traces, therefore, we seek to characterise the limit cycles and fixed points of our system of equations. We first generalize the un-normalized MD equations to

$$\frac{d\mathcal{E}}{d\tau} = (\mathcal{N} - a_1\mathcal{E} - a_2 d^2 \mathcal{N}^4 - a_3 V_{ZF}^2 - a_3 V_{SF}^2)\mathcal{E}, \quad (1)$$

$$\frac{dV_{ZF}}{d\tau} = \left(\frac{b_{1Z}\mathcal{E}}{1 + b_{2Z}d^2\mathcal{N}^4} - b_{3Z}\right)V_{ZF}, \quad (2)$$

$$\frac{dV_{SF}}{d\tau} = \left(\frac{b_{1S}\mathcal{E}}{1 + b_{2S}d^2\mathcal{N}^4} - b_{3S}\right)V_{SF}, \quad (3)$$

$$\frac{d\mathcal{N}}{d\tau} = -(c_1\mathcal{E} + c_2)\mathcal{N} + q(\tau). \quad (4)$$

This model encompasses drift wave turbulence level $\mathcal{E}$, drift wave driving temperature gradient $\mathcal{N}$, zonal flow velocity V_{ZF}, streamer flow velocity V_{SF}, and the heating rate q which is a control parameter of the system. This model thus extends, to the case when zonal flows are joined by streamers, the key physics encapsulated in the description in Ref. 46: "When the drift wave turbulence drive becomes sufficiently strong to overcome flow damping, it generates zonal flows by Reynolds stress. Drift wave turbulence and zonal flows then form a self-regulating system as the shearing by zonal flows damps the drift wave turbulence." We note that this model follows the approach expressed in Eq. (17) of MD,[21] in that the zonal flows and streamers do not explicitly enter the time evolution equation for the temperature gradient, Eq. (4). The zonal flows and streamers are indirectly coupled to each other through the evolving temperature gradient and microturbulence level. To maximise mathematical congruence with the model of MD, there is no direct cross term in $V_{SF}V_{ZF}$. We note that our introduction of streamers into this model is mathematically symmetric with the approach to zonal flows expressed in the model of Ref. 21. This reflects our emphasis in this paper on the question of mathematical robustness: we have two predators rather than one, operating on the same mathematical footing. A corollary is that in the present model, neither the zonal flows nor the streamers explicitly enter the time evolution equation for the temperature gradient, Eq. (4). In reality, one might assume that the streamers, unlike the zonal flows, when active can relax the temperature gradient to some extent.

The corresponding normalized equations are

$$\frac{dE}{dt} = (N - N^4 - E - U_1 - U_2)E, \tag{5}$$

$$\frac{dU_1}{dt} = \nu_1\left(\frac{E}{1 + \zeta N^4} - \eta_1\right)U_1, \tag{6}$$

$$\frac{dU_2}{dt} = \nu_2\left(\frac{E}{1 + \zeta N^4} - \eta_2\right)U_2, \tag{7}$$

$$\frac{dN}{dt} = q - (\rho + \sigma E)N. \tag{8}$$

Here, we have defined normalized variables

$$N = a_2^{1/3}\mathcal{N}, \quad E = a_1 a_2^{1/3}\mathcal{E}, \quad U_1 = a_2^{1/3}a_3 V_{ZF}^2,$$
$$U_2 = a_2^{1/3}a_3 V_{SF}^2, \quad t = a_2^{-1/3}\tau,$$

and the transformed model parameters are

$$\nu_1 = \frac{2b_{1Z}}{a_1}, \quad \nu_2 = \frac{2b_{1S}}{a_1}, \quad \eta_1 = \frac{b_{3Z}}{b_{1Z}}a_1 a_2^{1/3}, \quad \eta_2 = \frac{b_{3S}}{b_{1S}}a_1 a_2^{1/3},$$
$$\rho = c_2 a_2^{1/3}, \quad \sigma = \frac{c_1}{a_1}, \quad \zeta = \frac{b_{2Z}}{a_2^{4/3}}, \quad b_{2Z} = b_{2S},$$
$$q(t) = a_2^{2/3}q(\tau), \quad d = 1.$$

This rescaling of variables differs from that in MD, where Eqs. (13) and (14) are rescaled using $t = a_2^{1/3}\tau$ as indicated in MD, whereas Eq. (12) appears to have been rescaled

inconsistently, using $t = a_2^{-1/3}\tau$, which is the scaling applied to all four model equations in the present paper. There appear to be no consequences for the results in MD. The system of Eqs. (5)–(8) thus generalizes the system of Eqs. (15)–(17) of MD by introducing two distinct flow variables, U_1 and U_2, to replace the single zonal flow variable U. We refer to U_1 as zonal flow, U_2 as streamer flow.

Section III of this paper addresses transition phenomenology given time-independent coefficients, as characterised primarily by time traces. This requires careful comparison with the specific scenarios identified in Figs. 2–4 of MD. The MD scenarios predetermine the choice of parameter values and initial conditions that we consider. We typically probe neighbouring phase space by considering in addition eighty-one (three to the fourth power) nearby phase trajectories. In Sec. IV, we consider the phase space evolution of our system and establish comparisons between the MD model and ours. In Sec. V, we analyse possible links to the phenomenology of tokamak plasmas, in the spirit of MD and II.

III. MODELLING CONFINEMENT TRANSITIONS

In the limit where either one of the two parameters that represent distinct classes of coherent nonlinear structures (zonal flows or streamers) in our model vanishes, it reproduces exactly the results shown in Fig. 2 of MD, as required. Figure 1 displays the corresponding results for the case where both streamers and zonal flows exist. In the nomenclature of MD, the system starts from an overpowered state near H-mode, with negligible turbulence E and large scale structures U_1, U_2. The eventual growth of turbulence accompanies a sharp drop in N to unstable L-mode, while also providing energy for U_1 and U_2. Drift wave turbulence is later suppressed and the maximum amplitude of large scale flows declines, leaving only the mean flow to support the transport barrier.[19] Finally, the stable T-mode, which combines a steady-state level of E with lower N than H-mode, appears after the oscillating transition regime. During this transition, energy is extracted from the initially dominant oscillating streamer flow U_2 to the zonal flow U_1 until the former vanishes.

In Fig. 2, we plot the system evolution for the case where the values of ν_2 and η_2 are different from Fig. 1, while all other parameter values are identical. Specifically, in Fig. 1 $\nu_2/\nu_1 = \eta_2/\eta_1 = 1.01$, whereas in Fig. 2 $\nu_2/\nu_1 = 0.01$ and $\eta_2/\eta_1 = 0.1$. This weakens both the drive and the damping of structures U_2 compared to zonal flows U_1 in Fig. 2, with respect to the case of Fig. 1. Before time reaches $t \sim 6000$, the evolution is very similar to Fig. 2 of MD. However, at $t \sim 6500$ we find a dramatic change. A limit cycle appears after the long-term fixed point time series. The amplitudes of U_1 and U_2 exchange rather fast compared to Fig. 1. Furthermore, the period of the limit cycle is rather long: several hundred time units. With the appearance of zonal flows and streamers, the T-mode becomes unstable.

Figure 3 shows the case where the heating rate is higher than for Fig. 1, $q = 0.58$, but all other model parameters are the same. At each pulsed occurrence of zonal flows U_1 and streamers U_2, the former extract energy from the latter,
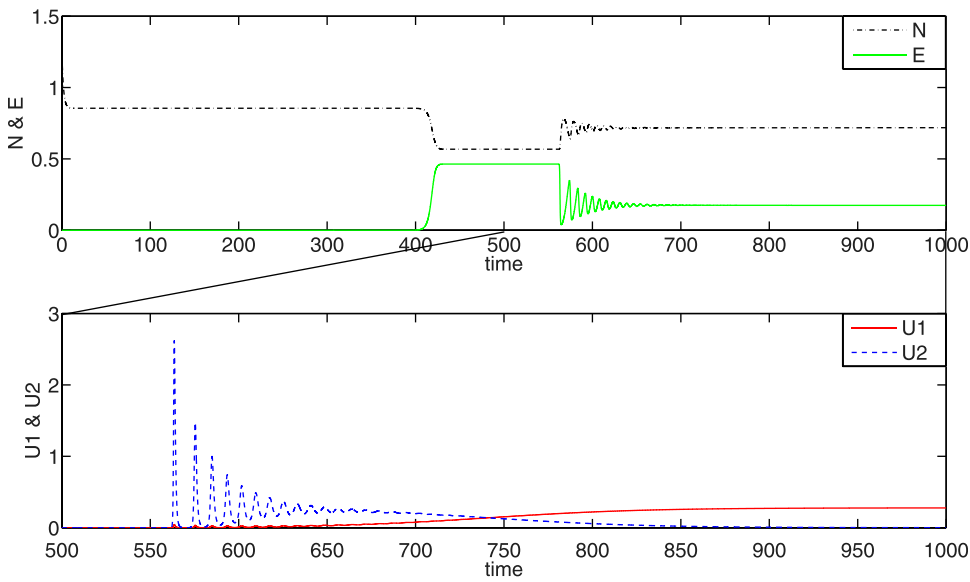
FIG. 1. Upper panel: From overpowered H-mode to unstable L-mode then to T-mode. Lower panel: Transition to T-mode for U_1 and U_2 showing intersection at $t \simeq 750$ followed by energy reversal. The parameters are $\nu_1 = 19$, $\nu_2 = 1.01\nu_1$, $\eta_1 = 0.12$, $\eta_2 = 1.01\eta_1$, $q = 0.47$, $\rho = 0.55$, $\sigma = 0.6$, $\zeta = 1.7$.
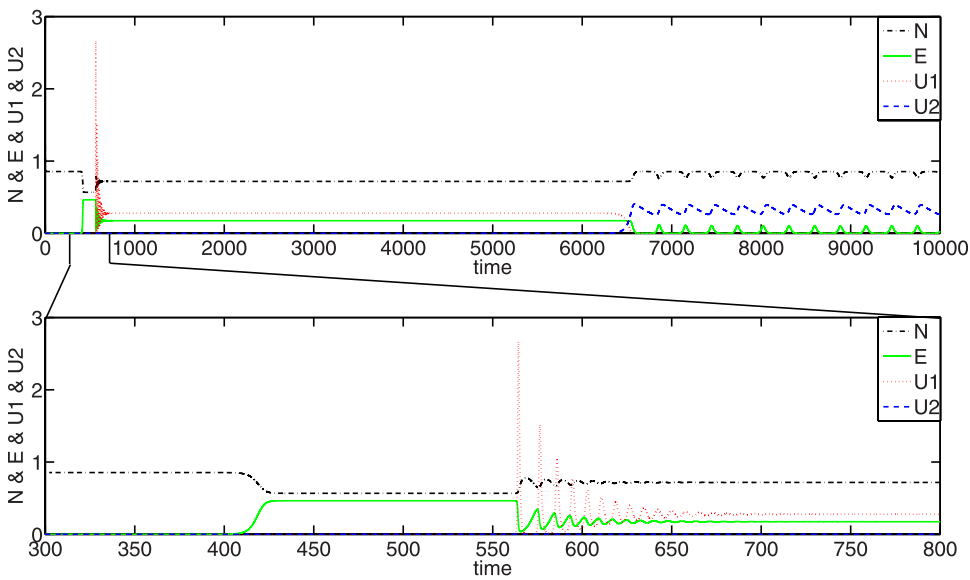

FIG. 2. Upper panel: Transition from stable fixed point state to unstable oscillatory limit cycle state. Lower panel: Zoom in version from $t = 300$ to $t = 800$. The parameters are $\nu_1 = 19$, $\nu_2 = 0.01\nu_1$, $\eta_1 = 0.12$, $\eta_2 = 0.1\eta_1$, $q = 0.47$, $\rho = 0.55$, $\sigma = 0.6$, $\zeta = 1.7$.
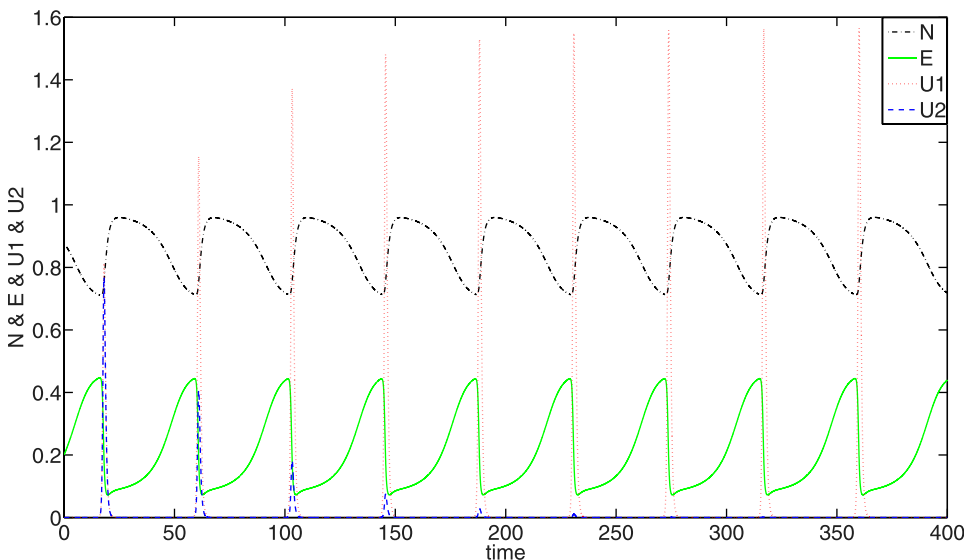

FIG. 3. Energy transfer from U_2 to U_1 during pulses of strong nonlinear oscillation, followed by limit cycle oscillation in N, E and U_1. The parameters are $\nu_1 = 19$, $\nu_2 = 1.01\nu_1$, $\eta_1 = 0.12$, $\eta_2 = 1.01\eta_1$, $q = 0.58$, $\rho = 0.55$, $\sigma = 0.6$, $\zeta = 1.7$.
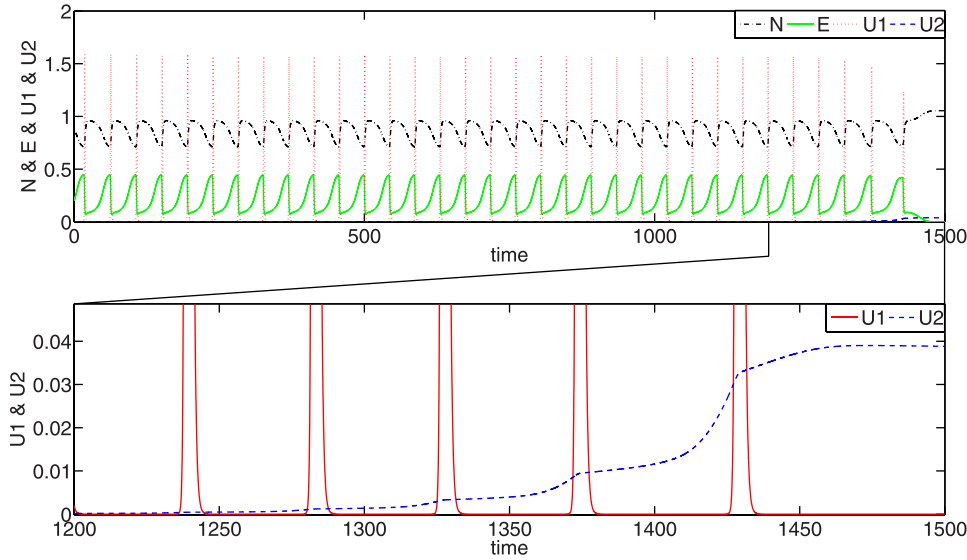
FIG. 4. Upper panel: Collapse of limit cycle in N, E, and U_1. Lower panel: Stair increasing of U_2. The parameters are $\nu_1 = 19$, $\nu_2 = 0.01\nu_1$, $\eta_1 = 0.12$, $\eta_2 = 0.01\eta_1$, $q = 0.58$, $\rho = 0.55$, $\sigma = 0.6$, $\zeta = 1.7$.

which become extinct after the sixth pulse. Thereafter, there are limit cycle oscillations in E, N, and U_1 equivalent to the limit cycle for E, N, and U in the case in MD.

Figure 4 shows time traces for the case where all parameters, except the heating rate $q = 0.58$ which is the same as in Fig. 3, are those of Fig. 2. Together with Fig. 5, where the heating rate q is slightly increased to $q = 0.582$ instead of $q = 0.58$, this enables us to relate our model to Fig. 4 of MD, which showed that if in MD $q = 0.582$ instead of 0.58, the limit cycle eventually collapses after many oscillations. The final state has N finite and the remaining variables are zero; this is designated the QH-mode fixed point in MD. The corresponding cases for our model Eqs. (5)–(8) are shown in Figs. 4 and 5. A precursor to limit cycle collapse is apparent in Fig. 4 in the growth of the streamer field U_2 during the episodes of zonal flow quiescence in the last few oscillations of the system.

For the slightly different parameter set used to generate Fig. 5, the pulses of U_1 and U_2 grow and die together. Their peak amplitude increases at each successive cycle, as does the time interval between them. At the final oscillation, U_1

and U_2 collapse promptly together, whereas E survives longer until it is extinguished by damping. The phenomenology of Fig. 5 thus corresponds more closely to that of Fig. 4 of MD, compared to our Fig. 4.

Figure 6 illustrates how system evolution towards the finite-N final state of Fig. 5 depends on the damping rate η_2 of streamers. We fix all parameters except η_2 and find that, with increasing η_2, there are more peaks of U_2 correlating with cyclic growth of E, which acts as a damping sink of N. Successive peaks increase in height prior to extinction, which results in a final state similar to Fig. 5.

IV. PHASE SPACE EVOLUTION

The time traces of the individual variables, plotted in Figs. 1–6, represent projections of the evolution in four-dimensional phase space of the system defined by Eqs. (5)–(8). In the present section, we capture the global phase space explored by this system, for parameter values corresponding, or adjacent, to those used to generate Figs. 1–6. This approach enables us to identify and characterise the
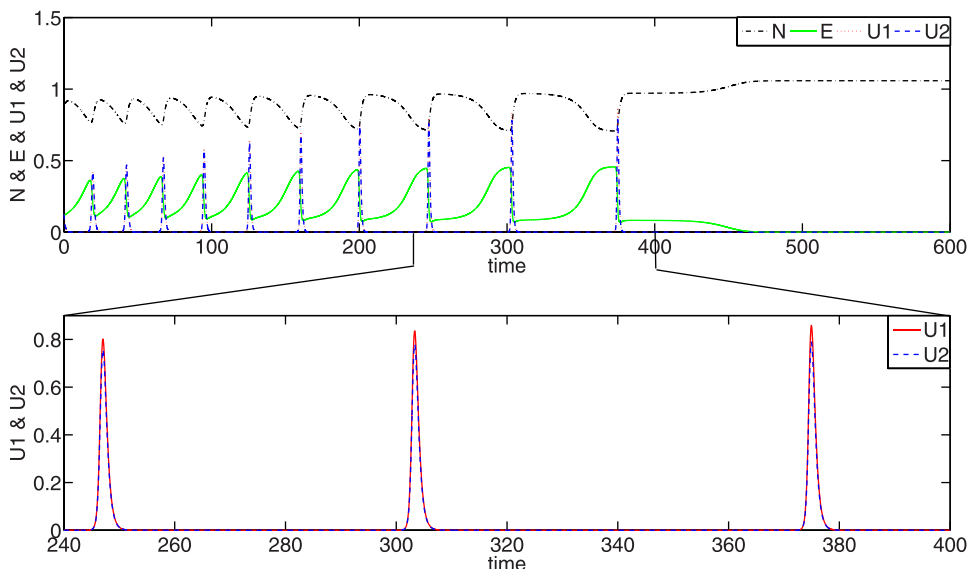

FIG. 5. Upper panel: Collapse of limit cycle with positively correlated growth of pulses of U_1 and U_2. Lower panel: Zoom in version from $t = 240$ to $t = 400$. The parameters are $\nu_1 = 19$, $\nu_2 = 1.0001\nu_1$, $\eta_1 = 0.12$, $\eta_2 = 1.0001\eta_1$, $q = 0.582$, $\rho = 0.55$, $\sigma = 0.6$, $\zeta = 1.7$.
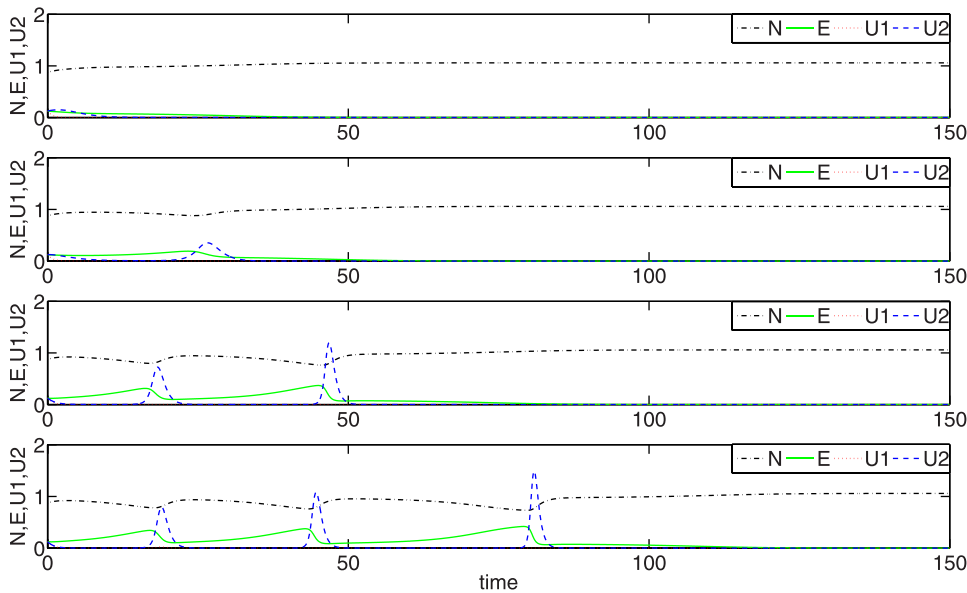
FIG. 6. Evolution to the finite N attractor for different values of η_2. Upper panel: $\eta_2 = 0.05$. Middle upper panel: $\eta_2 = 0.06$. Middle lower panel: $\eta_2 = 0.10$. Lower panel: $\eta_2 = 0.11$. The remaining parameters are the same: $\nu_1 = 19$, $\nu_2 = 1.001\nu_1$, $\eta_1 = 0.12$, $q = 0.582$, $\rho = 0.55$, $\sigma = 0.6$, $\zeta = 1.7$.

nature of initial and final states and of the transitional behaviour between them. The relationship between these figures is summarized in Table I. These results are supplemented in the Appendix by stability studies. At issue are two main physical concerns, which map directly to the properties of different energy confinement regimes in tokamaks, insofar as the zero-dimensional approach and the identifications made in MD, for example, may be valid. First, what is the nature of the final state that is reached at long times? For example, is it an attractive fixed point or a limit cycle (implying a nearby repulsive fixed point)? Second, there is the question, discussed previously, of robustness of three-variable models against the inclusion of a fourth variable (here, streamers) in the model. For example, the pioneering work of MD includes identification of a limit cycle (Fig. 3 of MD) with a specific confinement regime. Is this limit cycle—and, proceeding by analogy, the confinement regime that it represents—stable against the presence of streamers in addition to zonal flows?

Figure 7 displays the generalisation, to the four-variable system, of the case of the three-variable system addressed in Fig. 2 of MD. To fix ideas, the two left-hand plots correspond to the three-variable case for the parameters of Fig. 2 of MD, showing the attractive fixed point which has finite values of E, N, and U. The inward spiral path of the system from a random initial position is shown, both in (E, N, U) space and projected onto the (E, U) plane. It is evident that this path lies on a topological structure in phase space, whose dimensionality is lower by one than that of the full phase space. The two right-

hand plots of Fig. 7 show how this system changes when the two variables U_1 and U_2 replace U, for the parameter values used to generate the traces in Fig. 1, which are adjacent to those for Fig. 2 of MD, as discussed above. The centre right-hand plot shows initial spiral convergence in (E, U_2) which closely resembles that in the (E, U) plane displayed at centre left. Whereas with three variables this convergence is towards a fixed point, the existence of a fourth variable renders this attractive fixed point unstable. In consequence, the final stage of system evolution consists of injection in the U_1 direction to a fixed point at finite (E, N, U_1) with $U_2 = 0$. The far right plot in Fig. 7 demonstrates that this is indeed a fixed point, towards which phase space evolution originating from eighty-one different initial points converges. In each case, there is spiral convergence on a manifold followed by injection along U_1. The choice of initial condition affects only the orientation of this convergence manifold with respect to U_1 and U_2. We note also that the final state with finite U_1 differs from the MD final state for which $U = 0$.

Figure 8 illustrates the phase space evolution of the system whose time traces are plotted in Fig. 2, which like Fig. 7 is a case with parameters adjacent to those used to generate Fig. 2 of MD. The initial spiral convergence in the (E, U_1) plane, shown in the centre panel, resembles that in the (E, U) plane for the MD case plotted in the left panel, which is identical to the centre-left panel of Fig. 7. As in Fig. 7, the stable fixed point of the three-variable system is unstable for the four-variable system, for which there is injection along U_2. Unlike Fig. 7, where this injection is towards a stable fixed
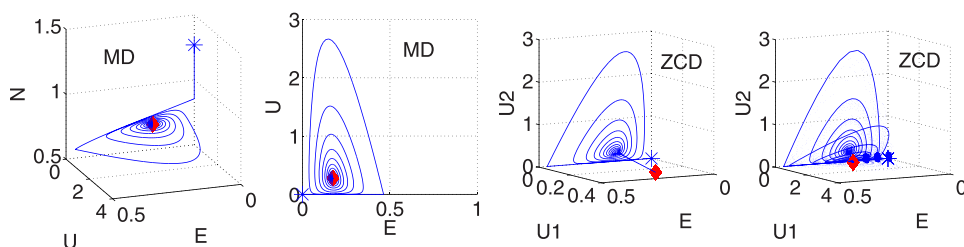

FIG. 7. First panel: Fig. 2 in MD. The parameters are $\nu = 19$, $\eta = 0.12$, $q = 0.47$, $\rho = 0.55$, $\sigma = 0.6$, $\zeta = 1.7$. Second panel: Projection of first panel on E-U plane. Third panel: Phase plot of Fig. 1. Last panel: Phase plot of Fig. 1 with 81 initial conditions. Stars denote initial values, blue dots denote trajectories and red diamonds denote final states.

FIG. 8. First panel: Projection of Fig. 2 in MD on E-U plane. The parameters are $\nu = 19$, $\eta = 0.12$, $q = 0.47$, $\rho = 0.55$, $\sigma = 0.6$, $\zeta = 1.7$. Second panel: Phase plot of Fig. 2. Last panel: Phase plot of Fig. 2 with 81 initial conditions. Stars denote initial values, blue dots denote trajectories and red diamonds denote final states.
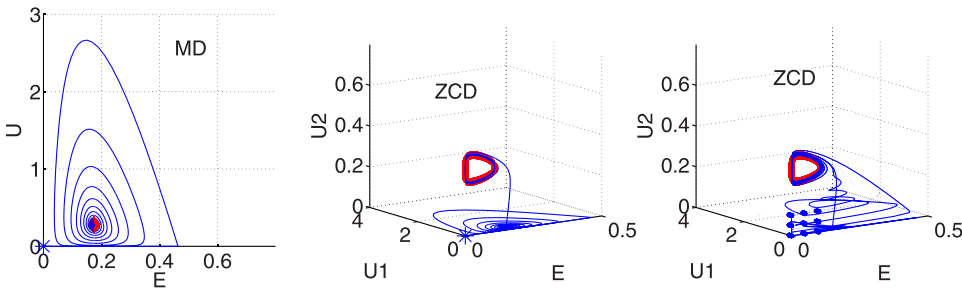
point, in Fig. 8 the injection is onto a stable limit cycle that has finite slow oscillations in (N, E, U_2) with $U_1 = 0$ in the four-variable system.

The three-variable MD system has a limit cycle in (N, E, U) for the case shown in Fig. 3 of MD. This is re-plotted in the two left panels of Fig. 9 and in the left panel of Fig. 10. Figures 9 and 10 relate to the time traces shown in Figs. 3 and 4 of this paper, obtained for parameter sets for the four-variable system which are adjacent to those used in MD for the three-variable system. For the parameters of Fig. 9, which is the phase space plot for Fig. 3, it is clear from the

two right-hand panels that the limit cycle behaviour is essentially that of the MD system. The transient evolution towards the limit cycle involves circulation on similar planes that have successively lower peak values of U_2. The final limit cycle in (N, E, U_1), with $U_2 = 0$, is essentially that in (N, E, U) for the three-variable system.

The three-variable MD attractive limit cycle which manifests in the four-variable system as shown in Fig. 9 is, however, unstable. Figure 10, which is the phase space plot for Fig. 4, shows that the system leaves the former limit cycle and transiently explores the additional phase space dimension
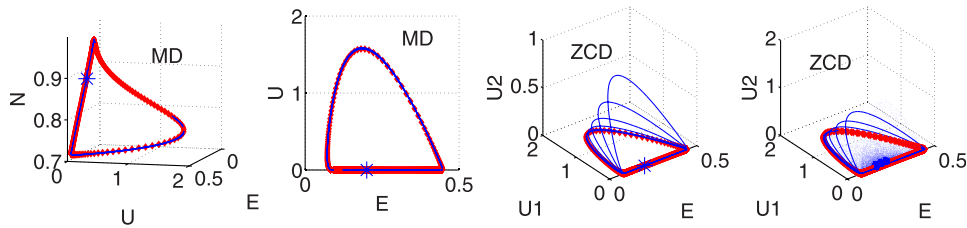

FIG. 9. First panel: Fig. 3 in MD. The parameters are $\nu = 19$, $\eta = 0.12$, $q = 0.58$, $\rho = 0.55$, $\sigma = 0.6$, $\zeta = 1.7$. Second panel: Projection of first panel on E-U plane. Third panel: Phase plot of Fig. 3 here ZCD. Last panel: Phase plot of Fig. 3 here ZCD with 81 initial conditions. Stars denote initial values, blue dots denote trajectories and red diamonds denote final states.
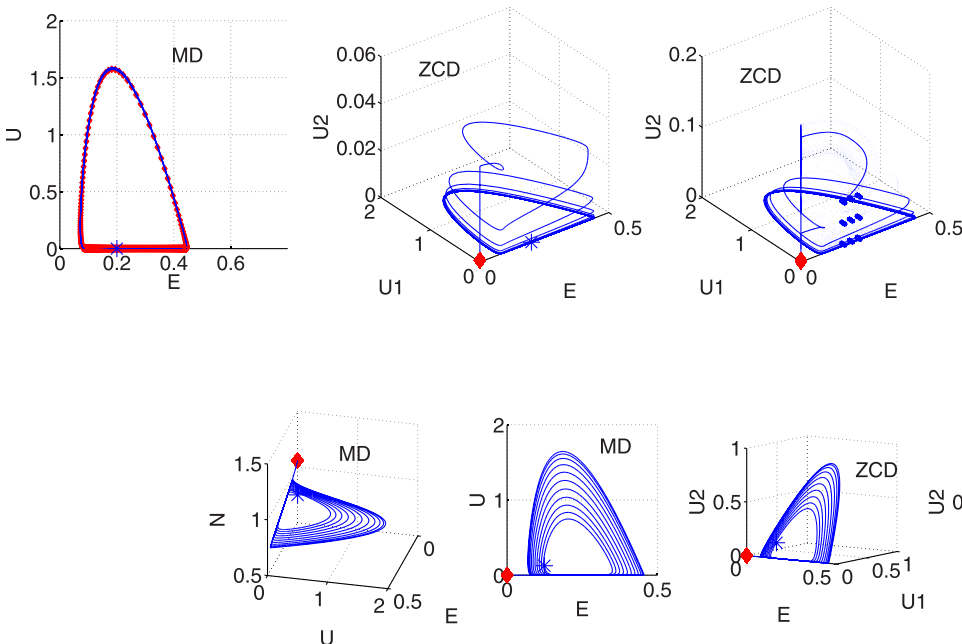
FIG. 10. First panel: Projection of Fig. 3 in MD on E-U plane. The parameters are $\nu = 19$, $\eta = 0.12$, $q = 0.58$, $\rho = 0.55$, $\sigma = 0.6$, $\zeta = 1.7$. Middle panel: Phase plot of Fig. 4 here. Last panel: Phase plot of Fig. 4 here with 81 initial conditions. Stars denote initial values, blue dots denote trajectories and red diamonds denote final states.

FIG. 11. First panel: Phase plot for Fig. 4 of MD. Second panel: Projection of Fig. 4 in MD on E-U plane. The parameters are $\nu = 19$, $\eta = 0.12$, $q = 0.582$, $\rho = 0.55$, $\sigma = 0.6$, $\zeta = 1.7$. Third panel: Phase plot of Fig. 5 here. Last panel: Phase plot of Fig. 5 here with 81 initial conditions. Stars denote initial values, blue dots denote trajectories and red diamonds denote final states.
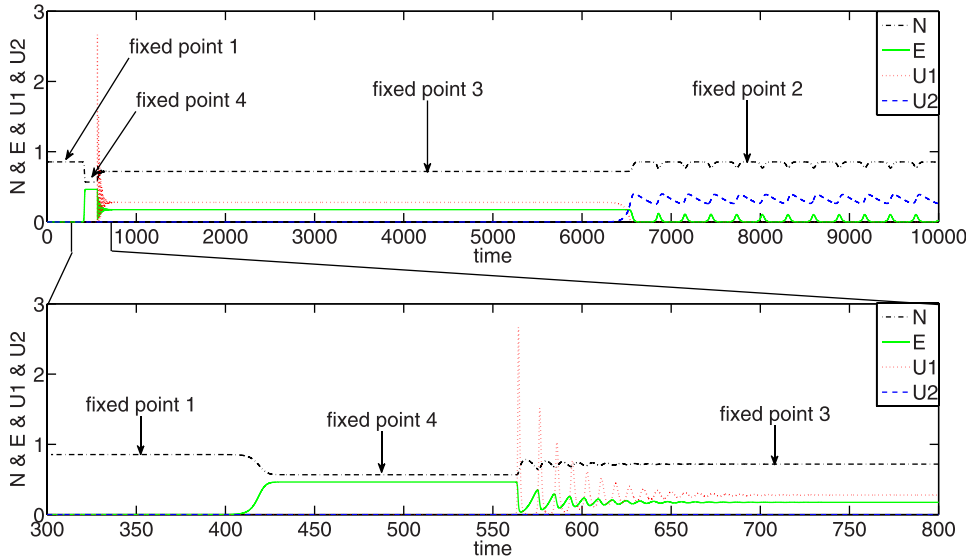
FIG. 12. Time series of Fig. 2 in this paper, annotated in light of Fig. 13.

associated with the additional variable, before converging to a new fixed point that has N finite and all other variables zero. This class of attractive fixed point is noted in Fig. 4 of MD, shown in the far left panel of Fig. 11 and, projected on the (E, U) plane, in the centre left panel. The two right-hand panels of Fig. 11 are the phase space plots for Fig. 5, showing convergence to the origin in (E, U_1, U_2) space while N remains finite. The final step to the origin is preceded by circulation around and away from an apparent repulsive fixed point with finite values of E, U_1 and U_2. The far right panel of Fig. 11 shows that the choice of initial conditions merely affects the orientation in (U_1, U_2) space of the plane of this transient circulation.

The phase space behaviour discussed thus far assists us in re-visiting the time traces in Fig. 2, for which the corresponding phase plot is given in Fig. 13. In Fig. 12, we annotate Fig. 2 in light of Fig. 13. These two figures demonstrate how, for the four-variable system, the T-mode of the three-variable system becomes unstable at long times. The system

then evolves towards the newly identified attractive limit cycle in (N, E, U_2). Here, slow oscillations in N correlate with those in U_2, both of which remain finite throughout, while bursts of E, feeding on U_2, occur between extinctions.

V. CONCLUSIONS

Contemporary experimental results from the DIII-D[31] and HL-2A tokamaks[32] reinforce the relevance of zero-dimensional predator-prey models to transitions between energy confinement regimes. Understanding how the outputs of related, but different, predator-prey models for plasma confinement phenomenology may resemble or deviate from each other is therefore important. In this paper, we have focused on the consequences of adding a second predator, and hence a fourth field variable, to the three-field MD[21] model. Quantitative studies have been presented for parameter sets that are maximally adjacent to those in MD, which yield the time traces shown in Figs. 1–6 and 12. These are projections of the phase space dynamics shown in Figs. 7–11 and 13 (Table I). It is found that both congruences and deviations can occur between the three-field and four-field models. For example, Fig. 10 shows how a limit cycle in the three-field system is unstable for four fields in the relevant parameter range, where the attractor is a fixed point. Conversely, Fig. 8 shows a three-field fixed point mapping to a four-field limit cycle. Figure 13 shows the complex, but resolved, phase space dynamics underlying a generalisation to four fields of the three-field scenario modelled in Fig. 2 of MD. We conclude that exploration of the linkages between different
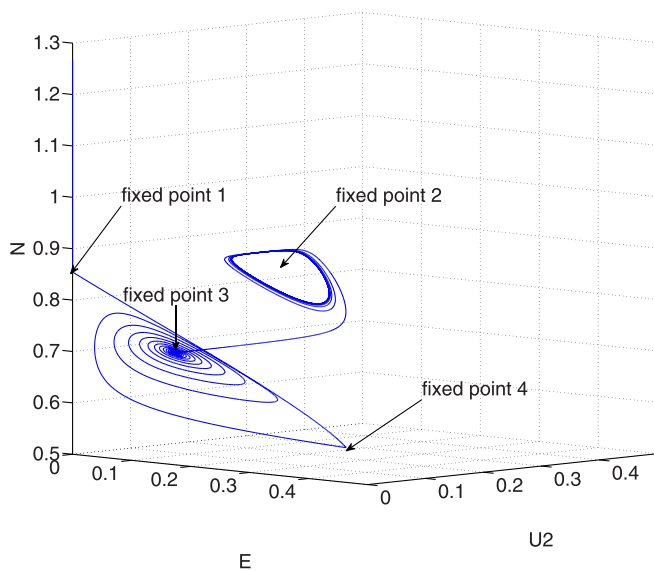
FIG. 13. Phase plot of Fig. 2 in this paper.

TABLE I. Summary of Figs. 1–11.

Case	q	ν_2/ν_1	η_2/η_1	Timetraces	Phaseplot	Manifold
1	0.47	1.01	1.01	Fig. 1	Fig. 7	Fixed point
2	0.47	0.01	0.1	Fig. 2	Fig. 8	Limit cycle
3	0.58	1.01	1.01	Fig. 3	Fig. 9	Limit cycle
4	0.58	0.01	0.01	Fig. 4	Fig. 10	Limit cycle
5	0.582	1.0001	1.0001	Fig. 5	Fig. 11	Fixed point
6	0.582	1.001	0.05; 0.06; 0.1; 0.11	Fig. 6	N/A	N/A

zero-dimensional models, capturing full phase space properties so far as computationally possible, needs to keep pace with the continuing development and refinement of individual zero-dimensional models in fusion plasma physics.

Zero-dimensional models remain attractive because they embody physically motivated narratives that may account for global fusion plasma confinement phenomenology. Ideally, the end states (attractors) of zero-dimensional models, together with the transitional behaviour en route from the initial configurations, should be robustly identifiable with fusion plasma confinement states and transitions. Zero-dimensional predator-prey models, constructed in terms of a small number of variables representing global quantities such as the drift wave turbulence level $\mathcal{E}$, drift wave driving temperature gradient $\mathcal{N}$, zonal flow velocity V_{ZF}, streamer flow velocity V_{SF}, and the heating rate q in Eqs. (1)–(4), are intrinsically nonlinear. This nonlinearity implies the potential for a rich and varied set of attractors and transitional behaviour, together with strong dependence on the numerical values of model parameters. The present paper has taken steps to explore this potential for the model of interest in the case of parameter sets close to those studied previously in MD, with a view to strengthening the links between families of zero-dimensional models on the one hand, and fusion plasma confinement phenomenology on the other. We note finally that some of the considerations addressed here may carry over to other fields where it is hoped to develop zero-dimensional models that have descriptive, or even predictive, power for global phenomena in macroscopic multiscale driven-dissipative systems. A topical instance is provided by zero-dimensional modelling in climate science, see for example Ref. 47 and references therein, where some general circulation models incorporate Lotka-Volterra features.[48]

ACKNOWLEDGMENTS

APPENDIX: IDENTIFICATION AND STABILITY OF FIXED POINTS

We start from Eqs. (5) to (8), and for simplicity define the normalized equations as

$$
\begin{cases}
dE/dt = (N - N^4 - E - U_1 - U_2)E \equiv f(E, U_1, U_2, N) \\
dU_1/dt = \nu_1 \left(\dfrac{E}{1 + \zeta N^4} - \eta_1 \right) U_1 \equiv g_1(E, U_1, N) \\
dU_2/dt = \nu_2 \left(\dfrac{E}{1 + \zeta N^4} - \eta_2 \right) U_2 \equiv g_2(E, U_2, N) \\
dN/dt = q - (\rho + \sigma E)N \equiv h(E, N).
\end{cases}
\tag{A1}
$$

We regard point $(N_0, E_0, U_{10}, U_{20})$ as a fixed point of the 4D system and define

$$
\begin{cases}
f_0 \equiv f(E_0, U_{10}, U_{20}, N_0), \\
g_{10} \equiv g_1(E_0, U_{10}, N_0) \\
g_{20} \equiv g_2(E_0, U_{20}, N_0) \\
h_0 \equiv h(E_0, N_0).
\end{cases}
\tag{A2}
$$

By construction $f_0 = g_{10} = g_{20} = h_0 = 0$. Near the fixed point, we make a local linear expansion of the model parameters

$$
\triangle E \equiv E - E_0; \quad \triangle U_1 \equiv U_1 - U_{10}; \quad \triangle U_2 \equiv U_2 - U_{20};
$$
$$
\triangle N \equiv N - N_0.
\tag{A3}
$$

This gives rise to the linearized equations

$$
\begin{cases}
f \approx f_0 + \dfrac{\partial f}{\partial E} \triangle E + \dfrac{\partial f}{\partial U_1} \triangle U_1 + \dfrac{\partial f}{\partial U_2} \triangle U_2 + \dfrac{\partial f}{\partial N} \triangle N \\
g_1 \approx g_{10} + \dfrac{\partial g_1}{\partial E} \triangle E + \dfrac{\partial g_1}{\partial U_1} \triangle U_1 + \dfrac{\partial g_1}{\partial N} \triangle N \\
g_2 \approx g_{20} + \dfrac{\partial g_2}{\partial E} \triangle E + \dfrac{\partial g_2}{\partial U_2} \triangle U_2 + \dfrac{\partial g_2}{\partial N} \triangle N \\
h \approx h_0 + \dfrac{\partial h}{\partial E} \triangle E + \dfrac{\partial h}{\partial N} \triangle N.
\end{cases}
\tag{A4}
$$

To obtain the eigenvalues of the system, we calculate the corresponding Jacobian matrix

$$
J = \begin{pmatrix}
\dfrac{\partial}{\partial E} f & \dfrac{\partial}{\partial U_1} f & \dfrac{\partial}{\partial U_2} f & \dfrac{\partial}{\partial N} f \\
\dfrac{\partial}{\partial E} g_1 & \dfrac{\partial}{\partial U_1} g_1 & \dfrac{\partial}{\partial U_2} g_1 & \dfrac{\partial}{\partial N} g_1 \\
\dfrac{\partial}{\partial E} g_2 & \dfrac{\partial}{\partial U_1} g_2 & \dfrac{\partial}{\partial U_2} g_2 & \dfrac{\partial}{\partial N} g_2 \\
\dfrac{\partial}{\partial E} h & \dfrac{\partial}{\partial U_1} h & \dfrac{\partial}{\partial U_2} h & \dfrac{\partial}{\partial N} h
\end{pmatrix}_{(E_0, \ U_{10}, \ U_{20}, \ N_0)}.
\tag{A5}
$$

We now identify the fixed points.
① If $E = 0$,

$$
\begin{cases}
N - N^4 - E - U_1 - U_2 = K \\
U_1 = 0 \\
U_2 = 0 \\
N = \dfrac{q}{\rho},
\end{cases}
\tag{A6}
$$

where K is a constant that can take any value.
② If $E \neq 0$,

$$
\begin{cases}
N - N^4 - E - U_1 - U_2 = 0 \\
\left(\dfrac{E}{1 + \zeta N^4} - \eta_1 \right) U_1 = 0 \\
\left(\dfrac{E}{1 + \zeta N^4} - \eta_2 \right) U_2 = 0 \\
q - (\rho + \sigma E)N = 0.
\end{cases}
\tag{A7}
$$

From the second and third equations in this group, it follows that U_1 and U_2 cannot be non-zero simultaneously.

TABLE II. MD system.

MD	Fixed points	Eigenvalues	Property
Fig. 2	$E = 0$; $U = 0$; $N = 0.8545$	$-2.28; -0.55; 0.3213$	Saddle point-Index 1
	$E = 0.1742$; $U = 0.2780$; $N = 0.7181$	$-0.0360 \pm 0.8099i; -0.7567$	Spiral node (**final state**)
	$E = 0.4638$; $U = 0$; $N = 0.5675$	$-0.6460 \pm 0.0963i; 5.2111$	Inward spiral and source
Fig .3	$E = 0$; $U = 0$; $N = 0.8545$	$-2.28; -0.55; -0.1821$	Node
	$E = 0.2249$; $U = 0.1077$; $N = 0.8468$	$0.0069 \pm 0.4991i; -0.9236$	Outward spiral and sink (**limit cycle**)
	$E = 0.0769$; $U = 0$; $N = 0.9729$	$0.0969; -0.7700; -1.7010$	Saddle point-Index 1
	$E = 0.4588$; $U = 0$; $N = 0.7028$	$3.8817; -0.3122; -0.9718$	Saddle point-Index 1
Fig. 4	$E = 0$; $U = 0$; $N = 1.0582$	$-2.28; -0.55; -0.1957$	Node (**final state**)
	$E = 0.2260$; $U = 0.1036$; $N = 0.8489$	$0.0080 \pm 0.4892i; -0.9275$	Outward spiral and sink
	$E = 0.0825$; $U = 0$; $N = 0.9708$	$0.1002; -0.7821; -1.6558$	Saddle point-Index 1
	$E = 0.4576$; $U = 0$; $N = 0.7058$	$3.8348; -0.3058; -0.9764$	Saddle point-Index 1

TABLE III. ZCD system.

ZCD	Fixed points	Eigenvalues	Property
Fig. 7	$E = 0$; $U_1 = 0$; $U_2 = 0$; $N = 0.8545$	$-2.28; -0.55; 0.3213; -2.3258$	4D Saddle point-Index 1
	$E = 0.1757$; $U_1 = 0$; $U_2 = 0.2770$; $N = 0.7171$	$-0.0365 \pm 0.8165i; -0.7581; 0.0228$	Inward spiral, source and sink
	$E = 0.1742$; $U_1 = 0.2780$; $U_2 = 0$; $N = 0.7187$	$-0.0360 \pm 0.8099i; -0.0230; -0.7567$	Spiral node (**final state**)
	$E = 0.4638$; $U_1 = 0$; $U_2 = 0$; $N = 0.5675$	$-0.6460 \pm 0.0963i; 5.2402; 5.2111$	Inward spiral and sources
Fig. 8	$E = 0$; $U_1 = 0$; $U_2 = 0$; $N = 0.8545$	$-2.28; -0.55; 0.3213; -0.0023$	4D Saddle point-Index 1
	$E = 0.0219$; $U_1 = 0$; $U_2 = 0.3275$; $N = 0.8346$	$0.0019 \pm 0.0272i; -0.5888; -2.052$	Outward spiral and sinks (**limit cycle**)
	$E = 0.1742$; $U_1 = 0.2780$; $U_2 = 0$; $N = 0.7187$	$-0.0360 \pm 0.8099i; 0.0205; -0.7567$	Inward spiral, source and sink
	$E = 0.4638$; $U_1 = 0$; $U_2 = 0$; $N = 0.5675$	$-0.6460 \pm 0.0963i; 0.0726; 5.2111$	Outward spiral and sources
Fig. 9	$E = 0$; $U_1 = 0$; $U_2 = 0$; $N = 1.0545$	$-2.28; -0.55; -2.3258; -0.1821$	Node
	$E = 0.2265$; $U_1 = 0$; $U_2 = 0.1078$; $N = 0.8456$	$0.0062 \pm 0.5045i; 0.0228; -0.9248$	Outward spiral, source and sink
	$E = 0.2249$; $U_1 = 0.1077$; $U_2 = 0$; $N = 0.8468$	$0.0069 \pm 0.4991i; -0.0230; -0.9236$	Outward spiral and sinks (**limit cycle**)
	$E = 0.0769$; $U_1 = 0$; $U_2 = 0$; $N = 0.9729$	$0.0969; -0.7700; -1.7010; -1.741$	4D Saddle point-Index 1
	$E = 0.4588$; $U_1 = 0$; $U_2 = 0$; $N = 0.7028$	$-0.3122; -0.9718; 3.8817; 3.8975$	4D Saddle point-Index 2
Fig. 10	$E = 0$; $U_1 = 0$; $U_2 = 0$; $N = 1.0545$	$-2.28; -0.55; -0.1821; -0.0002$	Node (**final state**)
	$E = 0.2249$; $U_1 = 0.1077$; $U_2 = 0$; $N = 0.8468$	$0.0069 \pm 0.4990i; 0.0226; -0.9236$	Outward spiral, source and sink
	$E = 0.4588$; $U_1 = 0$; $U_2 = 0$; $N = 0.7028$	$-0.3122; -0.9718; 3.8817; 0.0614$	4D Saddle point-Index 2
	$E = 0.0769$; $U_1 = 0$; $U_2 = 0$; $N = 0.9729$	$0.0969; 0.0056; -0.7700; -1.7010$	4D Saddle point-Index 2
Fig. 11	$E = 0$; $U_1 = 0$; $U_2 = 0$; $N = 1.0582$	$-2.28; -0.55; -2.2805; -0.1957$	Node (**final state**)
	$E = 0.2260$; $U_1 = 0$; $U_2 = 0.1036$; $N = 0.8489$	$0.0080 \pm 0.4892i; 0.0002; -0.9275$	Outward spiral, source and sink
	$E = 0.2260$; $U_1 = 0.1036$; $U_2 = 0$; $N = 0.8489$	$0.0080 \pm 0.4892i; -0.0002; -0.9275$	Outward spiral and sinks
	$E = 0.0825$; $U_1 = 0$; $U_2 = 0$; $N = 0.9708$	$0.1002; -0.7821; -1.6558; -1.6562$	4D Saddle point-Index 1
	$E = 0.4576$; $U_1 = 0$; $U_2 = 0$; $N = 0.7058$	$-0.3058; -0.9764; 3.8348; 3.8349$	4D Saddle point-Index 2

(ii)   If $U_1 = 0$, $U_2 \neq 0$, $E \neq 0$,

$$\begin{cases} N - N^4 - E - U_1 - U_2 = 0 \\ \dfrac{E}{1 + \zeta N^4} - \eta_1 = K \\ \dfrac{E}{1 + \zeta N^4} - \eta_2 = 0 \\ q - (\rho + \sigma E)N = 0, \end{cases} \tag{A8}$$

(ii)   If $U_1 \neq 0$, $U_2 = 0$, $E \neq 0$,

$$\begin{cases} N - N^4 - E - U_1 - U_2 = 0 \\ \dfrac{E}{1 + \zeta N^4} - \eta_1 = 0 \\ \dfrac{E}{1 + \zeta N^4} - \eta_2 = K \\ q - (\rho + \sigma E)N = 0, \end{cases} \tag{A9}$$

where K is a constant that can take any value.

(iii)   If $U_1 = U_2 = 0$, $E \neq 0$,

$$\begin{cases} N - N^4 - E = 0 \\ U_1 = 0 \\ U_2 = 0 \\ q - (\rho + \sigma E)N = 0. \end{cases} \tag{A10}$$

Solutions for the specific cases of the MD and ZCD systems considered in this paper are shown in Tables II and III.

[1]A. Hasegawa and M. Wakatani, Phys. Rev. Lett. **59**, 1581 (1987).
[2]S. Coda, M. Porkolab, and K. H. Burrell, Phys. Rev. Lett. **86**, 4835 (2001).
[3]M. Jakubowski, R. J. Fonck, and G. R. McKee, Phys. Rev. Lett. **89**, 265003 (2002).
[4]G. R. McKee et al., Phys. Plasma **10**, 1712 (2003).
[5]G. D. Conway, B. D. Scott, J. Schirmer, M. Reich, A. Kendl, and ASDEX Upgrade team, Plasma Phys. Controlled Fusion **47**, 1165 (2005).

[6]P. H. Diamond, S.-I. Itoh, K. Itoh, and T. S. Hahm, Plasma Phys. Controlled Fusion **47**, R35 (2005).

[7]D. K. Gupta, R. J. Fonck, G. R. McKee, D. J. Schlossberg, and M. W. Schafer, Phys. Rev. Lett. **97**, 125002 (2006).

[8]T. Yamada, S.-I. Itoh, T. Maruta, N. Kasuya, Y. Nagashima, S. Shinohara, K. Terasaka, M. Yagi, S. Inagaki, Y. Kawai, A. Fujisawa, and K. Itoh, Nature Phys. **4**, 721 (2008).

[9]W. Dorland, F. Jenko, M. Kotschenreuther, and B. N. Rogers, Phys. Rev. Lett. **85**, 5579 (2000).

[10]F. Jenko, W. Dorland, M. Kotschenreuther, and B. N. Rogers, Phys. Plasmas **7**, 1904 (2000).

[11]P. H. Diamond and Y. B. Kim, Phys. Fluids B **3**, 1626 (1991).

[12]F. Wagner *et al.*, Phys. Rev. Lett. **49**, 1408 (1982).

[13]G. Manfredi, C. M. Roach, and R. O. Dendy, Plasma Phys. Controlled Fusion **43**, 825 (2001).

[14]J. Q. Li, Y. Kishimoto, N. Miyato, T. Matsumoto, and J. Q. Dong, Nucl. Fusion **45**, 1293 (2005).

[15]N. Kasuya, M. Yagi, K. Itoh, and S.-I. Itoh, Phys. Plasmas **15**, 052302 (2008).

[16]A. Fujisawa, Plasma Phys. Controlled Fusion **53**, 124015 (2011).

[17]G. R. Tynan, A. Fujisawa, and G. McKee, Plasma Phys. Controlled Fusion **51**, 113001 (2009).

[18]F. Wagner, Plasma Phys. Controlled Fusion **49**, B1 (2007).

[19]P. H. Diamond, A. Hasegawa, and K. Mima, Plasma Phys. Controlled Fusion **53**, 124001 (2011).

[20]E. J. Doyle *et al.*, Nucl. Fusion **47**, S18 (2007).

[21]M. A. Malkov and P. H. Diamond, Phys. Plasmas **16**, 012504 (2009).

[22]J.-N. Leboeuf, L. A. Charlton, and B. A. Carreras, Phys. Fluids B **5**, 2959 (1993).

[23]P. H. Diamond, Y.-M. Liang, B. A. Carreras, and P. W. Terry, Phys. Rev. Lett. **72**, 2565 (1994).

[24]J. Hofbauer and J. W.-H. So, Appl. Math. Lett. **7**, 59 (1994).

[25]N. H. Bian and O. E. Garcia, Phys. Plasmas **10**, 4696 (2003).

[26]J. C. Sprott, J. C. Wildenberg, and Y. Azizi, Chaos, Solitons Fractals **26**, 1035 (2005).

[27]J. A. Vano, J. C. Wildenberg, M. B. Anderson, J. K. Noel, and J. C. Sprott, Nonlinearity **19**, 2391 (2006).

[28]N. H. Bian, Phys. Plasmas **17**, 044501 (2010).

[29]S.-I. Itoh and K. Itoh, Plasma Phys. Controlled Fusion **53**, 015008 (2011).

[30]K. Miki and P. H. Diamond, Nucl. Fusion **51**, 103003 (2011).

[31]L. Schmitz *et al.*, Phys. Rev. Lett. **108**, 155002 (2012).

[32]M. Xu, G. R. Tynan, P. H. Diamond *et al.*, Phys. Rev. Lett. **108**, 245001 (2012).

[33]N. W. Watkins, S. C. Chapman, R. O. Dendy, and G. Rowlands, Geophys. Res. Lett. **26**, 2617, doi:10.1029/1999GL900586 (1999).

[34]P. H. Diamond and T. S. Hahm, Phys. Plasmas **2**, 3640 (1995).

[35]D. E. Newman *et al.*, Phys. Plasmas **3**, 1858 (1996).

[36]B. A. Carreras *et al.*, Phys. Rev. Lett. **80**, 4438 (1998).

[37]R. O. Dendy and P. Helander, Phys. Rev E **57**, 3641 (1998).

[38]S. C. Chapman, R. O. Dendy, and G. Rowlands, Phys. Plasmas **6**, 4169 (1999).

[39]S. C. Chapman, R. O. Dendy, and B. Hnat, Phys. Rev. Lett. **86**, 2814 (2001).

[40]I. Gruzinov, P. H. Diamond, and M. N. Rosenbluth, Phys. Rev. Lett. **89**, 255001 (2002).

[41]S. C. Chapman, N. W. Watkins, R. O. Dendy, P. Helander, and G. Rowlands, Geophys. Res. Lett. **25**, 2397, doi:10.1029/98GL51700 (1998).

[42]D. Hughes, M. Paczuski, R. O. Dendy, P. Helander, and K. G. McClements, Phys. Rev. Lett. **90**, 131101 (2003).

[43]R. O. Dendy, S. C. Chapman, and M. Paczuski, Plasma Phys. Controlled Fusion **49**, A95 (2007).

[44]H. Haken, *Synergetics* (Springer, New York, 1977).

[45]H. G. Schuster, *Deterministic Chaos* (Physik-Verlag, Weinhein, 1984).

[46]E.-J. Kim and P. H. Diamond, Phys. Rev. Lett. **90**, 185006 (2003).

[47]A. V. Eliseev and I. I. Mokhov, Theor. Appl. Climatol. **89**, 9 (2007).

[48]P. M. Cox *et al.*, Nature **408**, 184 (2000).